IEEE Access
Multidisciplinary ⋮ Rapid Review ⋮ Open Access Journal

Received May 18, 2021, accepted June 5, 2021, date of publication June 14, 2021, date of current version June 30, 2021.

Digital Object Identifier 10.1109/ACCESS.2021.3089253

Drone Mobile Networks: Performance Analysis Under 3D Tractable Mobility Models

JIAYI HUANG[1], JIE TANG[1,2], (Senior Member, IEEE), ARMAN SHOJAEIFARD[3], (Senior Member, IEEE), ZHEN CHEN[1], (Member, IEEE), JUNCHENG HU[4], DANIEL KA CHUN SO[5], (Senior Member, IEEE), AND KAI-KIT WONG[6], (Fellow, IEEE)

[1]School of Electronic and Information Engineering, South China University of Technology, Guangzhou 510641, China
[2]National Mobile Communications Research Laboratory, Southeast University, Nanjing 210096, China
[3]BT Labs, Ipswich IP5 3RE, U.K.
[4]School of Humanity and Management, Guilin Medical University, Guilin 541100, China
[5]School of Electrical and Electronic Engineering, The University of Manchester, Manchester M13 9PL, U.K.
[6]Department of Electronic and Electrical Engineering, University College London, London WC1E 6BT, U.K.

Corresponding authors: Jie Tang (eejtang@scut.edu.cn) and Juncheng Hu (jc.hu@glmc.edu.cn)

This work was supported in part by the National Key Research and Development Project under Grant 2019YFB1804100, in part by the National Natural Science Foundation of China under Grant 61971194, in part by the Key Research and Development Project of Guangdong Province under Grant 2019B010156003, in part by the Natural Science Foundation of Guangdong Province under Grant 2019A1515011607, in part by the National Mobile Communications Research Laboratory, Southeast University, through the Open Research Fund, under Grant 2019D06, in part by the Fundamental Research Funds for the Central Universities under Grant 2019JQ08, and in part by the Guangdong Key Laboratory of Aerospace Communication and Networking Technology through the Research Fund Program under Grant 2018B030322004.

ABSTRACT Reliable wireless communication networks are a significant but challenging mission for post-disaster areas and hotspots in the era of information. However, with the maturity of unmanned aerial vehicle (UAV) technology, drone mobile networks have attracted considerable attention as a prominent solution for facilitating critical communications. This paper provides a system-level analysis for drone mobile networks on a finite three-dimensional (3D) space. Our aim is to explore the fundamental performance limits of drone mobile networks taking into account practical considerations. Most existing works on mobile drone networks use simplified mobility models (e.g., fixed height), but the movement of the drones in practice is significantly more complicated, which leads to difficulties in analyzing the performance of the drone mobile networks. Hence, to tackle this problem, we propose a stochastic geometry-based framework with a number of different mobility models including a random Brownian motion approach. The proposed framework allows to circumvent the extremely complex reality model and obtain upper and lower performance bounds for drone networks in practice. Also, we explicitly consider certain constraints, such as the small-scale fading characteristics relying on line-of-sight (LOS) and non line-of-sight (NLOS) propagation, and multi-antenna operations. The validity of the mathematical findings is verified via Monte-Carlo (MC) simulations for various network settings. In addition, the results reveal some design guidelines and important trends for the practical deployment of drone networks.

INDEX TERMS Drone mobile networks, mobility models, performance boundary, stochastic geometry theory, system-level analysis.

I. INTRODUCTION

The exponential growth of wireless data driven by mobile devices (e.g., tablets) has promoted the need for non-terrestrial networks [1]. However, it's a challenging task for operators to provide data services in special use-cases and circumstances such as large-gatherings (e.g., competitions) and man-made or natural disasters (e.g., earthquake). The latter in particular, is unpredictable by nature and has critical effects in terms of both ecological and economic costs. Securing communications capability is a vital component for disaster relief and response [2]. However, the conventional cellular communication systems are difficult to provide stable and reliable network connectivity. In the past few years,

The associate editor coordinating the review of this manuscript and approving it for publication was Hayder Al-Hraishawi.

drone technology has matured and widely used in smart city construction, such as security monitoring, real-time video streaming [3]. The drone can be quickly deployed by carrying a wireless communication module to form a drone air base station, thereby alleviating network congestion in hotspots [4], [5]. Drone opens up the possibility for rapid restoration of damaged cellular system. Drone assisted network is considered as a potential scheme for improving conventional terrestrial cellular networks, so it has received considerable attention in both industry and academia recently. Field experiments show that the air base station can effectively improve the user experience in the area with poor coverage and achieve the change of throughput from valley-to-peak [6]. The results shown that the UAV-based solution can provide stable network access capabilities compared to conventional systems in the scenario of large-scale gatherings and terrestrial communication infrastructure being destroyed. Therefore, current fifth generation (5G) and future integrated sixth generation (6G) wireless network also consider the application of UAVs in the system [7]. While there is no doubt about the advantages of UAVs, it still has some challenges for large-scale applications.

The stochastic theory is an approach widely used in the analysis of wireless networks because it can well capture the connection distance and randomness between nodes in many scenarios. The wrok in [8] used stochastic theory to study device-to-device (D2D) communications in post-disaster area. In [9], the authors borrowed tools from stochastic theory to modeling the channel in high-speed railway scenarios. The authors studied the coverage probability of low-earth-orbit satellites using stochastic geometry tools in [10]. The authors used stochastic geometry approach to describe the cache-enabled heterogeneous networks (HetNets) in [11]. Zhang *et al.* [12] analyzed the performance of cellular networks with cooperative relays using tools provided by stochastic geometry. The optimization of non-orthogonal multiple access (NOMA) in massive machine-type communications via stochastic theory has been studied in [13]. The authors evaluated the performance of full-duplex cooperative NOMA networks using stochastic geometry tools in [14]. The system coverage probability of UAV networks with the blockage effect using stochastic tools has been studied in [15]. In [16], the authors combined NOMA and full-duplex to solve the scarce of spectrum in UAV network using stochastic approach. The 3D-UAV enabled networks based on stochastic geometry as well as air-to-ground (A2G) channel modeling are studied in [17], and various effects such as the impact of shadowing in [18], [19] or the adoption of point process for modeling the UAVs distribution in [20], [21] are investigated. In [22], the authors analyzed the A2G channel model based on stochastic tools, where the 3D arbitrary trajectory changed.

Several studies on the performance of drone cellular networks based on stochastic geometry have also been reported in the literature. The downlink coverage probability was obtained ignoring LOS and NLOS propagation in [23]. In [24], the authors investigated the impact of Nakagami-m and LOS propagation in drone networks ignoring NLOS propagation. In [25], the authors studied the single drone MIMO networks where NLOS propagation was considered. In [26], the authors studied the coverage probability of static drone networks at a certain height considering LOS and NLOS propagation. In [27], the single drone network was investigated with considering a single slope path loss model where the drone could move to certain points. The single drone moving cyclically along the cell edge was studied based on stochastic geometry in [28]. The performance of multiple drone networks with hovering flight drone and cruising drone was studied in [29]. In [30], the authors compared the performance of sub-6 GHz and millimeter wave (mmWave) under drone hovering case. In [31], the authors investigated coverage probability of energy-harvesting-powered drones in 3D space with randomly deployed drones between maximum and minimum height. The 3D space drone cellular network is simplified to 2D plane by distributing UAVs at fixed height in [32].

A. CONTRIBUTIONS

In contrast to the drone networks considering either LOS or NLOS propagation in [23]–[25] and simplified drone mobility model (e.g., hovering, cruising, fixed height, static) in [27]–[32], we consider LOS and NLOS propagation with random mobility model in drone cellular networks. Although some random mobility models in HetNets have been provided in [33]–[36], the random mobility model of drone cellular networks has not been extensively studied. The main obstacle is the complex analysis of random mobility model, especially the Markov mobility model (i.e., the realistic mobility model [37]). Motivated by the above works, we present an analytical framework for the finite 3D drone mobile networks based on stochastic geometry. In this framework, we use the 3D Brownian motion and deterministic motion model to obtain performance boundaries of realistic drone mobile networks. Also, by considering LOS and NLOS propagation, a closed-form expression for spectral efficiency (SE) and outage probability of different mobility models including a random (Brownian) model are consequently provided. The main contributions of this paper can be summarized as follows:

- We provide a system-level analysis of the drone mobile networks, and the closed-form expressions of signal-to-interference-plus-noise ratio (SINR), SE and outage probability are derived. Also, we explicitly account for small-scale and large-scale fading characteristics relying on LOS and NLOS propagation and multi-slope path-loss.
- Instead of applying the complex Markov mobility model, we use the 3D Brownian motion and deterministic motion model to obtain performance boundaries of realistic drone mobile networks. The proposed framework allows for the study of drone mobile networks

under a number of mobility models including a random Brownian) motion model.
- Theoretical results are validated through MC simulations. The results show that the key features of drone mobile networks, in terms of high number of antennas and lower transmit power.

B. PAPER ORGANIZATION

The remainder of this paper is organized as follows. In Section II, the system description is given and a number of mobility models are presented. The spectrum efficiency and outage probability analysis of drone mobile network are provided in Section III. Numerical results are presented in Section IV, and finally, conclusions are provided in Section V.

Notation: $\boldsymbol{x}$ denotes a vector; Pr[.] denotes the probability; $\mathbb{E}_x[.]$ indicates the expectation; $\mathcal{F}_x[.]$ indicates the cumulative distribution function (CDF); $\mathcal{P}_x[.]$ denotes the probability density function (PDF); $\mathcal{M}_x[.]$ illustrates the m.g.f.; $|x|$ denotes the modulus; $\|\boldsymbol{x}\|$ indicates the Euclidean norm; $\mathcal{L}_x[.]$ denotes the Laplace transform (LT) function; $\mathbf{I}_{(.)}$ is the identity matrix; $\delta(.)$ indicates the Delta function; $\mathcal{H}(.)$ indicates the Heaviside step function; $\mathcal{G}(\kappa, \theta)$ denotes the Gamma distribution with shape parameter κ and scale parameter θ; $\mathcal{N}(\mu, \sigma^2)$ denotes the Gaussian distribution with mean μ and variance σ^2; $\Gamma(.)$ and $\Gamma(.,.)$ are respectively the Gamma and incomplete (upper) Gamma functions.

II. SYSTEM DESCRIPTION

A. NETWORK TOPOLOGY

We consider a large-scale drone mobile network as shown in Fig. 1, where K base stations (BSs) (i.e., UAVs) are deployed on the finite 3D ball of radius R following a homogeneous poisson point process (PPP) Φ with spatial density λ. The PPP-based abstraction model is confirmed to be a reliable approach for drone mobile networks. Let K_{LOS} and K_{NLOS} representing the number of drones under LOS and NLOS propagation (i.e., $K = K_{\mathrm{LOS}} + K_{\mathrm{NLOS}}$), respectively. Based on Slivnyak's theorem [38], and the stationary property of PPP, the analysis is carried for the typical user o supposed to be located at the origin.

B. PROPAGATION MODEL

In this network, the drones are mounted with M antennas, and be assumed to serve a user at each resource block. The typical user equip with single antenna. We assume each transmitter drone has perfect knowledge of typical user channel. $\boldsymbol{h}_b^T \sim \mathcal{CN}(\mathbf{0}, \mathbf{I}_M)$ indicates the small-scale fading channel between user o and its serving drone b. Here, we utilize the Nakagami-m distributed to capture the small-scale fading for LOS propagation, and use the Rayleigh distributed (i.e., exp(1)) for NLOS propagation. Noted that the exponential distribution is a special case of Gamma distribution with $m = 1$, so the Nakagami-m parameter for NLOS propagation is $m_{\mathrm{N}} = 1$. In addition, η indicates the additive white Gaussian noise (AWGN) at the typical user, where the mean and variance σ^2 are zero.

Considering the drones apply conjugate-beamforming (CB) in downlink (DL) direction of communications, the intended small-scale fading channel power gains g_b (from the serving drone b) experiencing LOS and NLOS propagation follow the distribution $\mathcal{G}\left(m_{\mathrm{L}}M, \frac{1}{m_{\mathrm{L}}}\right)$ and $\mathcal{G}\left(M, \frac{1}{m_{\mathrm{N}}}\right)$, where m_{L} and m_{N} respectively denote the Nakagami-m parameter for LOS and NLOS. The interfering small-scale fading channel power gains g_i (from the transmitting drone i) experiencing LOS and NLOS propagation follow the distribution $\mathcal{G}\left(m_{\mathrm{L}}, \frac{1}{m_{\mathrm{L}}}\right)$ and $\mathcal{G}(1,1)$, respectively [39], [40]. Then, the two-slope path-loss function can be constructed as

$$L(r) = \begin{cases} \max\left(\beta_0, \beta_1 r^{-\alpha_{\mathrm{L}}}\right), & \text{LOS propagation} \\ \max\left(\beta_0, \beta_1 r^{-\alpha_{\mathrm{N}}}\right), & \text{NLOS propagation} \end{cases} \tag{1}$$

where α_{L} and α_{N} represent path-loss exponents for LOS and NLOS links respectively with $\alpha_{\mathrm{N}} > \alpha_{\mathrm{L}} > 2$. β_0 illustrates the minimum coupling loss, β_1 indicates a constant parameter, r denotes the distance. Here, $\beta_1 = \frac{1}{\epsilon}\left(\frac{c}{4\pi f_c}\right)^2$, where f_c denotes the carrier frequency, and c represents the speed of light. For LOS ($L_{\mathrm{LOS}}(r)$) and NLOS ($L_{\mathrm{NLOS}}(r)$) links, $\epsilon = \epsilon_{\mathrm{LOS}} = 1$ dB and $\epsilon = \epsilon_{\mathrm{NLOS}} = 20$ dB, respectively [41].

A commonly used distance-dependent ITU-R Umi LOS and NLOS model (referred to as 3GPP LOS and NLOS model) is given as (2). By using (2), the LOS probability can be obtained as follows

$$\Pr[\mathrm{LOS}, r] = \min\left(\frac{18}{r}, 1\right)\left(1 - e^{-\frac{r}{36}}\right) + e^{-\frac{r}{36}}. \tag{2}$$

The function of LOS probability can be expressed as the following simplified model, which approximates widely utilized 3GPP channel model [42]–[44].

$$\Pr\left[\mathrm{LOS}, r_{(.)} = r\right] = \begin{cases} 1, & r \in [0, \mathsf{D}) \\ 0, & r \in [\mathsf{D}, \mathsf{R}] \end{cases} \tag{3}$$

where D indicates the critical distance, $\Pr[\mathrm{NLOS}, r] = 1 - \Pr[\mathrm{LOS}, r]$. According to the independence of homogeneous PPP Φ, the drones are divided into two parts (i.e., LOS drones and NLOS drones). The average number of LOS and NLOS drones are $\bar{K}_{\mathrm{LOS}} = \frac{4}{3}\pi \mathsf{D}^3 \lambda$ and $\bar{K}_{\mathrm{NLOS}} = \frac{4}{3}\pi\left(\mathsf{R}^3 - \mathsf{D}^3\right)\lambda$, respectively [45].

C. CELLULAR ASSOCIATION

The cellular association strategy is the path-loss based strategy. Mathematically, this strategy is given as

$$L(r_b) = \arg\max\left(L(r_l)\right), \quad \forall l \in \Phi, \tag{4}$$

where $L(r_b)$ represents the path-loss of serving drone b, and $L(r_l)$ indicates the path-loss of the l-th drone.

In next subsection, we will discuss three drone mobility models. Actually, the realistic drone mobility trajectory should follow the Markov mobility model, but Markov mobility model does not offer tractability for mathematical analysis. Hence, in this paper, we propose drone mobility model

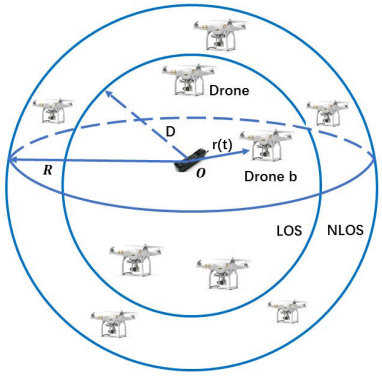

FIGURE 1. Depicting the finite 3D drone mobile network topology and propagation model with the path-loss based cellular association strategy.

(i.e., DM, 3D BM) to obtain upper and lower performance bounds for practical drone networks.

First, we discuss the CDF and PDF of $r_{b,\mathrm{LOS}}$ with uniformly-deployed under LOS case, where $r_{b,\mathrm{LOS}}$ denotes the distance between user o and its serving LOS drone.

Assuming K_{LOS} LOS drones (i.e., $K_{\mathrm{LOS}} > 0$) deployed on the finite 3D ball of radius D following uniformly distribution, the CDF and PDF of $r_{b,\mathrm{LOS}}$ are formulated as [46, Eqn. (6)]

$$\mathcal{F}_{r_{b,\mathrm{LOS}}}(r) = 1 - \left(1 - \frac{r^3}{\mathsf{D}^3}\right)^{K_{\mathrm{LOS}}}, \quad 0 \le r \le \mathsf{D} \tag{5}$$

and

$$\mathcal{P}_{r_{b,\mathrm{LOS}}}(r) = \frac{3\, r^2\, K_{\mathrm{LOS}}}{\mathsf{D}^3}\left(1 - \frac{r^3}{\mathsf{D}^3}\right)^{K_{\mathrm{LOS}}-1}, \quad 0 \le r \le \mathsf{D}. \tag{6}$$

Next, we aim to obtain the CDF and PDF of $r_{b,\mathrm{NLOS}}$ with uniformly-deployed under NLOS case, where $r_{b,\mathrm{NLOS}}$ denotes the distance between user o and its serving NLOS drone.

Assuming K_{NLOS} NLOS drones (i.e., $K_{\mathrm{LOS}} = 0$) deployed on the finite 3D ball double-bounded by radii R and D ($< \mathsf{R}$) following uniformly distribution, the CDF and PDF of $r_{b,\mathrm{NLOS}}$ are formulated as [47, Eqn. (3)]

$$\mathcal{F}_{r_{b,\mathrm{NLOS}}}(r) = 1 - \left(1 - \frac{r^3 - \mathsf{D}^3}{\mathsf{R}^3 - \mathsf{D}^3}\right)^{K_{\mathrm{NLOS}}}, \quad \mathsf{D} \le r \le \mathsf{R} \tag{7}$$

and

$$\mathcal{P}_{r_{b,\mathrm{NLOS}}}(r) = \frac{3\, r^2\, K_{\mathrm{NLOS}}}{\mathsf{R}^3 - \mathsf{D}^3}\left(1 - \frac{r^3 - \mathsf{D}^3}{\mathsf{R}^3 - \mathsf{D}^3}\right)^{K_{\mathrm{NLOS}}-1}, \quad \mathsf{D} \le r \le \mathsf{R}. \tag{8}$$

In this part, we obtain the CDF and PDF of $r_{b,\mathrm{LOS}}$ and $r_{b,\mathrm{NLOS}}$ with uniformly-deployed under LOS and NLOS case. Next part, we will consider the mobility model of the drones.

D. DRONE MOBILITY

We consider two case in 3D Brownian motion and deterministic motion mode. (i) At any given time, the distance between the mobile LOS drone and origin is smaller than D (i.e., $r_{\mathrm{LOS},j}(t) = \max\left(0, \min\left(\mathsf{D}, \hat{r}(t)\right)\right), j \in \{\mathrm{BM}, \mathrm{DM}\}$). (ii) At any given time, the distance between the mobile NLOS drone and origin is smaller than R and larger than D (i.e., $r_{\mathrm{NLOS},j}(t) = \max\left(\mathsf{D}, \min\left(\mathsf{R}, \hat{r}(t)\right)\right), j \in \{\mathrm{BM}, \mathrm{DM}\}$). In this network, the interfering drones are randomly generated in every time according to Poisson distributed in a 3D finite space. Also, because the cell association takes place in a slower time frame, once the user has been assigned a serving drone, it will be some time before the user changes the serving drone.

1) 3D BROWNIAN MOTION

In this subsection, we will analyze the mobility model 3D Brownian motion (BM) and deterministic motion (DM). In the mobility model, only the serving drone move, other interfering drones still fixed. The serving drone will move following the 3D BM model, the movement of the drone can be obtained according to the following stochastic differential equation (SDE) [48]

$$\mathrm{d}l(t) = v\, \mathrm{d}b(t) \tag{9}$$

where $l(t) = \{l_x(t), l_y(t), l_z(t)\}$ denotes a vector for the Cartesian coordinates at time t, $b(t) = \{b_x(t), b_y(t), b_z(t)\}$ indicates the Wiener process (i.e., standard BM) vector at time t, and v (i.e., representing average velocity) indicates a positive constant. Then, according to the characteristics of the Wiener process, we can obtain $b_x(t), b_y(t), b_z(t) \sim \mathcal{N}(0, t)$. $\hat{r}(t) = \sqrt{l_x^2(t) + l_y^2(t) + l_z^2(t)}$ is the corresponding Euclidean distance to the origin at time t. First, we will derive the CDF and PDF of $r_{\mathrm{LOS}}(t)$, where $r_{\mathrm{LOS}}(t)$ denotes the distance to the origin under LOS propagation at time t. Recall the mobility model for LOS drone under consideration, $r_{\mathrm{LOS},j}(t) = \max\left(0, \min\left(\mathsf{D}, \hat{r}(t)\right)\right)$. The CDF of $r_{\mathrm{LOS},j}(t)$ (a function of three variables) can be expressed as [49]

$$\mathcal{F}_{r_{\mathrm{LOS},j}(t)}(w) = \mathcal{F}_0(w)\, \mathcal{F}_{\min(\mathsf{D},\hat{r}(t))}(w), \tag{10}$$

where $\mathcal{F}_0(w)$ indicates the CDF of constant 0, and $\mathcal{F}_{\min(\mathsf{D},\hat{r}(t))}(w)$ represents the CDF of function $\min\left(\mathsf{D}, \hat{r}(t)\right)$. Based on the 3D BM, $\hat{r}(t) = \sqrt{l_x^2(t) + l_y^2(t) + l_z^2(t)}$. By solving the Fokker-Plank equation (FPE) based on satisfying the SDE in (9) and considering $b_x(t), b_y(t), b_z(t) \sim \mathcal{N}(0, t)$, we can obtain $l_x(t), l_y(t), l_z(t) \sim \mathcal{N}(0, 2\,vt)$. Hence, we can readily apply the Central Limit Theorem (CLT) to obtain $\hat{r}^2(t) \sim \mathcal{G}(\frac{3}{2}, 4\,vt)$. Then, $\hat{r}(t) \sim \mathrm{Nakagami}(\frac{3}{2}, 6\,vt)$. According to the characteristic of Nakagami-m distribution, the CDF and PDF can be directly given by

$$\mathcal{F}_{\hat{r}(t)}(w) = 1 - \frac{2}{\sqrt{\pi}}\Gamma\left(\frac{3}{2}, \frac{w^2}{4vt}\right) \tag{11}$$

and

$$\mathcal{P}_{\hat{r}(t)}(w) = \frac{w^2}{2\sqrt{\pi}\,(vt)^{\frac{3}{2}}} \exp\left(-\frac{w^2}{4vt}\right). \tag{12}$$

The CDF and PDF of x (a constant parameter), $\mathcal{F}_{\mathsf{x}}(w)$ and $\mathcal{P}_{\mathsf{x}}(w)$, are respectively given by

$$\mathcal{F}_{\mathsf{x}}(w) = \mathcal{H}(w - \mathsf{x}) \tag{13}$$

and

$$\mathcal{P}_{\mathsf{x}}(w) = \delta(w - \mathsf{x}). \tag{14}$$

Hence, we can arrive at the CDF and PDF expressions of $r_{\mathrm{LOS,BM}}(t)$ in (15) and (16), as shown at the bottom of the next page.

Considering the 3D BM mobility, the CDF and PDF of $r_{\mathrm{LOS,BM}}(t)$ (i.e., mobile LOS drone distance) are formulated as (15) and (16), respectively.

$$\mathcal{F}_{r_{\mathrm{LOS,BM}}(t)}(w) = \left(1 + \frac{2}{\sqrt{\pi}}\Gamma\left(\frac{3}{2}, \frac{w^2}{4\,vt}\right)(\mathcal{H}(w - \mathsf{D}) - 1)\right)\mathcal{H}(w) \tag{15}$$

Next, we will derive the CDF and PDF of $r_{\mathrm{NLOS,BM}}(t)$ based on the 3D BM mobility model, where $r_{\mathrm{NLOS,BM}}(t)$ indicates the distance to the origin under NLOS propagation at time t. Recall the mobility model for NLOS drone, $r_{\mathrm{NLOS,BM}}(t) = \max\left(\mathsf{D}, \min\left(\mathsf{R}, \hat{r}(t)\right)\right)$. We can express the corresponding CDF as [49]

$$\mathcal{F}_{r_{\mathrm{NLOS},j}(t)}(w) = \mathcal{F}_{\mathsf{D}}(w)\,\mathcal{F}_{\min(\mathsf{R},\hat{r}(t))}(w), \tag{17}$$

where $\mathcal{F}_{\mathsf{D}}(w)$ indicates the CDF of constant D, $\mathcal{F}_{\min(\mathsf{R},\hat{r}(t))}(w)$ represents the CDF of function $\min\left(\mathsf{R}, \hat{r}(t)\right)$.

In formula (11) and formula (13), we derived the probability distribution of $\mathcal{F}_{\hat{r}(t)}(w)$, $\mathcal{F}_{\mathsf{R}}(w)$ and $\mathcal{F}_{\mathsf{D}}(w)$. Hence, with some basic numerical steps, we can arrive at the CDF and PDF expressions of $r_{\mathrm{NLOS,BM}}(t)$ in (18) and (19), as shown at the bottom of the next page.

Considering the 3D BM mobility, the CDF and PDF of $r_{\mathrm{NLOS,BM}}(t)$ (i.e., mobile NLOS drone distance) are formulated as (18) and (19), respectively.

$$\mathcal{F}_{r_{\mathrm{NLOS,BM}}(t)}(w) = \left(1 + \frac{2}{\sqrt{\pi}}\Gamma\left(\frac{3}{2}, \frac{w^2}{4\,vt}\right)(\mathcal{H}(w - \mathsf{R}) - 1)\right)\mathcal{H}(w - \mathsf{D}) \tag{18}$$

Also, we can obtain the CDF and PDF for LOS and NLOS based on homogeneous PPP with density λ. The distribution of BM movement distance is equivalent to the distribution of the nearest drone distance following homogeneous PPP with density λ [48], and we can obtain the CDF of homogeneous PPP in (5), where $K_{\mathrm{LOS}} = \frac{4}{3}\pi\mathsf{D}^3\lambda$, so (5) is identical to (15) [48]. Then, by solving this equation, we can obtain the density for LOS as shown at the bottom of the next page (20). Also, a similar approach can be used to obtain the density for NLOS given in (21), as shown at the bottom of the next page.

2) DETERMINISTIC MOTION

In this part, the characteristic of the deterministic motion (i.e., moving towards a target at a constant speed) is studied. Once the transmission link has been established, the serving drone cannot move toward to other targets. The corresponding Euclidean distance to the origin (i.e., $t > 0$) can be given by

$$\hat{r}(t) = r_0 - vt \tag{22}$$

where v indicates a constant (e.g., representing velocity) and r_0 denotes the distance at time $t = 0$. It should be noted that a positive value v means same direction and vice versa. Then, we will derive the CDF and PDF of $r_{\mathrm{LOS,DM}}(t)$, where $r_{\mathrm{LOS,DM}}(t)$ indicates the distance to the origin under LOS propagation at time t. Recall the deterministic mobility model for LOS drone, $r_{\mathrm{LOS,DM}}(t) = \max\left(0, \min\left(\mathsf{D}, \hat{r}(t)\right)\right)$, where $\hat{r}(t) = r_0 - vt$. Consider $Y = \mathsf{a}X - \mathsf{b}$, where Y and X are random variables, and a and b are constants. Hence, based on this linear transformation, the PDF of Y is constructed as [30]

$$\mathcal{P}_Y(y) = \frac{1}{|\mathsf{a}|}\mathcal{P}_X\left(\frac{y - \mathsf{b}}{\mathsf{a}}\right). \tag{23}$$

Then, the CDF and PDF of $\hat{r}_{\mathrm{LOS}}(t)$ can be respectively formulated as

$$\mathcal{F}_{\hat{r}_{\mathrm{LOS}}(t)}(w) = 1 - \left(1 - \frac{(vt + w)^3}{\mathsf{D}^3}\right)^{K_{\mathrm{LOS}}} \tag{24}$$

and

$$\mathcal{P}_{\hat{r}_{\mathrm{LOS}}(t)}(w) = \frac{3(vt + w)^2\,K_{\mathrm{LOS}}}{\mathsf{D}^3}\left(1 - \frac{(vt + w)^3}{\mathsf{D}^3}\right)^{K_{\mathrm{LOS}} - 1} \tag{25}$$

The CDF and PDF of $\hat{r}_{\mathrm{NLOS}}(t)$ can be respectively formulated as

$$\mathcal{F}_{\hat{r}_{\mathrm{NLOS}}(t)}(w) = 1 - \left(1 - \frac{(vt + w)^3 - \mathsf{D}^3}{\mathsf{R}^3 - \mathsf{D}^3}\right)^{K_{\mathrm{NLOS}}} \tag{26}$$

and

$$\mathcal{P}_{\hat{r}_{\mathrm{NLOS}}(t)}(w) = \frac{3(vt + w)^2\,K_{\mathrm{NLOS}}}{\mathsf{R}^3 - \mathsf{D}^3}\left(1 - \frac{(vt + w)^3 - \mathsf{D}^3}{\mathsf{R}^3 - \mathsf{D}^3}\right)^{K_{\mathrm{NLOS}} - 1}. \tag{27}$$

Using the above, together with the aid of similar expression in (10) and (17), we can arrive at the results in (28) and (30).

Considering the deterministic motion mobility, the CDF and PDF of $r_{\mathrm{LOS,DM}}(t)$ are formulated in (28) and (29), as shown at the bottom of the next page.

$$\mathcal{F}_{r_{\mathrm{LOS,DM}}(t)}(w) = \mathcal{H}(w)\left(1 + (\mathcal{H}(w - \mathsf{D}) - 1)\left(1 - \frac{(vt + w)^3}{\mathsf{D}^3}\right)^{K_{\mathrm{LOS}}}\right) \tag{28}$$

Considering the deterministic motion mobility, the CDF and PDF of $r_{\mathrm{NLOS,DM}}(t)$ are formulated in (30) and (31), as shown at the bottom of the next page.

$$\mathcal{F}_{r_{\mathrm{NLOS,DM}}(t)}(w) = \mathcal{H}(w-\mathsf{D})\Bigg(1+(\mathcal{H}(w-\mathsf{R})-1) \times\Big(\frac{\mathsf{R}^3-(vt+w)^3}{\mathsf{R}^3-\mathsf{D}^3}\Big)^{K_{\mathrm{NLOS}}}\Bigg) \tag{30}$$

E. SINR FORMULATION

Using the formula above, the received SINR can be formulated as

$$\mathrm{SINR}=\frac{X}{I_{\mathrm{Iagg}}+\sigma^2} \tag{32}$$

where

$$X = pg_bL(r_b) \tag{33}$$

and

$$I_{\mathrm{Iagg}} = \sum_{i\in\Phi\setminus\{b\}} pg_iL(r_i) \tag{34}$$

with σ^2 and p used to indicate the noise variance and transmit power, respectively.

III. PERFORMANCE ANALYSIS

In this section, we will analysis the performances of spectral efficiency and outage probability.

First, the spectral efficiency (in nat/s/Hz) of the typical user is expressed as (35), as shown at the bottom of the next page [50], where $\Pr[\mathrm{LOS}, r=r_b]$ and $\Pr[\mathrm{NLOS}, r=r_b]$ denote the distance-dependent LOS and NLOS probabilities given in (3). $\mathcal{P}_{r_b}(r)$ and $\mathcal{F}_{\mathrm{SINR}|r_b=r}[\gamma]$ indicate the PDF of the transmitter-receiver distance (expressed in (6) and (8)), and the CDF of the SINR conditioned on $r_b=r$.

By using MGF methodlogy, the spectral efficiency of the typical user conditioned on transmitter-receiver distance r_b is obtained.

$$\mathbb{E}\left[\log(1+\mathrm{SINR})\right] = \int_0^R\int_0^{+\infty}\left[(1-\mathcal{M}_{\mathrm{X}|r_b}(z))\times\mathcal{M}_{\mathrm{Iagg}|r_b}(z)\right] \times\frac{\exp(-z\sigma^2)}{z}\mathcal{P}_{r_b}(r)\,\mathrm{d}z\mathrm{d}r \tag{36}$$

where $\mathcal{M}_{\mathrm{X}|r_b}(z)$ can be easily derived and $\mathcal{M}_{\mathrm{Iagg}|r_b}(z)$ can be obtained by the LT of aggregate interference. The $\mathcal{M}_{\mathrm{X}|r_b}(z)$ conditioned on LOS and NLOS are respectively given by

$$\mathcal{M}_{\mathrm{X}|r_b}(z) = \left(1+\frac{zpL(r_b)}{m_{\mathrm{L}}}\right)^{-Mm_{\mathrm{L}}} \tag{37}$$

$$\mathcal{P}_{r_{\mathrm{LOS,BM}}(t)}(w) = \left(1+\frac{2}{\sqrt{\pi}}\Gamma\left(\frac{3}{2},\frac{w^2}{4\,vt}\right)(\mathcal{H}(w-\mathsf{D})-1)\right)\delta(w) + \left(\frac{2}{\sqrt{\pi}}\Gamma\left(\frac{3}{2},\frac{w^2}{4\,vt}\right)\delta(w-\mathsf{D}) - \frac{w^2}{2\sqrt{\pi}\,(vt)^{\frac{3}{2}}}\exp\left(-\frac{w^2}{4\,vt}\right)(\mathcal{H}(w-\mathsf{D})-1)\right)\mathcal{H}(w). \tag{16}$$

$$\mathcal{P}_{r_{\mathrm{NLOS,BM}}(t)}(w) = \left(1+\frac{2}{\sqrt{\pi}}\Gamma\left(\frac{3}{2},\frac{w^2}{4\,vt}\right)(\mathcal{H}(w-\mathsf{R})-1)\right)\delta(w-\mathsf{D}) + \left(\frac{2}{\sqrt{\pi}}\Gamma\left(\frac{3}{2},\frac{w^2}{4\,vt}\right)\delta(w-\mathsf{R}) - \frac{1}{2\sqrt{\pi}w}\left(\frac{w^2}{vt}\right)^{\frac{3}{2}}\exp\left(-\frac{w^2}{4\,vt}\right)(\mathcal{H}(w-\mathsf{R})-1)\right)\mathcal{H}(w-\mathsf{D}). \tag{19}$$

$$\lambda = \frac{3\log\left(1-\frac{\mathcal{H}(w)}{\sqrt{\pi}}\left(2\mathcal{H}(w-\mathsf{D})\Gamma\left(\frac{3}{2},\frac{w^2}{4\,tv}\right)-2\Gamma\left(\frac{3}{2},\frac{w^2}{4\,tv}\right)+\sqrt{\pi}\right)\right)}{4\pi\mathsf{D}^3\log\left(1-\frac{w^3}{\mathsf{D}^3}\right)} \tag{20}$$

$$\lambda = \frac{3\log\left(1-\frac{\mathcal{H}(w-\mathsf{D})}{\sqrt{\pi}}\left(2\mathcal{H}(w-\mathsf{R})\Gamma\left(\frac{3}{2},\frac{w^2}{4\,tv}\right)-2\Gamma\left(\frac{3}{2},\frac{w^2}{4\,vt}\right)+\sqrt{\pi}\right)\right)}{4\pi\left(\mathsf{R}^3-\mathsf{D}^3\right)\log\left(1-\frac{w^3-\mathsf{D}^3}{R^3-\mathsf{D}^3}\right)}. \tag{21}$$

$$\mathcal{P}_{r_{\mathrm{LOS,DM}}(t)}(w) = \delta(w) + (\mathcal{H}(w)\,\delta(w-\mathsf{D}) + (\mathcal{H}(w-\mathsf{D})-1)\delta(w)\,)\left(1-\frac{(vt+w)^3}{\mathsf{D}^3}\right)^{K_{\mathrm{LOS}}} -\mathcal{H}(w)\,(\mathcal{H}(w-\mathsf{D})-1)\frac{3\,K_{\mathrm{LOS}}(vt+w)^2}{\mathsf{D}^3}\left(1-\frac{(vt+w)^3}{\mathsf{D}^3}\right)^{K_{\mathrm{LOS}}-1}. \tag{29}$$

and

$$\mathcal{M}_{\mathrm{X}|r_b}(z) = \left(1+\frac{zpL(r_b)}{m_{\mathrm{N}}}\right)^{-M}. \tag{38}$$

After deriving the expression of spectral efficiency, we will deduct the expression of outage probability.

The CDF of the SINR (outage probability) conditioned on $r_o = r$ is given by (39), as shown at the bottom of the next page, with (i) written using the identity $x^n f(x) \equiv (-1)^n \frac{\mathrm{d}^n}{\mathrm{d}s^n}\mathcal{L}_{f(x)}[s]$ (a property of LT function). Hence, the CDF of the SINR (outage probability) of the typical user can be expressed by (40), as shown at the bottom of the next page, where $\Pr[\mathrm{LOS}, r = r_b]$ and $\Pr[\mathrm{NLOS}, r = r_b]$ denote the distance-dependent LOS and NLOS probabilities given in (3).

Next, we will obtain the LT of the aggregate interference under LOS and NLOS propagation by invoking the probability generating functional (PGFL).

The LT of the aggregate interference under LOS and NLOS propagation are respectively given by

$$\begin{aligned}\mathscr{L}_{I_{\mathrm{LOS}}}[s] &= \mathbb{E}\left[\exp(-sI_{\mathrm{LOS}})\right]\\ &= \mathbb{E}\left[\exp\left(-s\sum_{i\in\Phi_{\mathrm{LOS}}\setminus\{b\}} pg_iL_{\mathrm{LOS}}(r_i)\right)\right]\\ &= \mathbb{E}_{\Phi_{\mathrm{LOS}}}\left[\prod_{i=1}^{K_{\mathrm{LOS}}}\frac{1}{\left(1+\frac{sp}{m_{\mathrm{L}}}L_{\mathrm{LOS}}(r_i)\right)^{m_{\mathrm{L}}}}\right]\\ &= \mathbb{E}_{r_i}\left[\left(\frac{1}{\left(1+\frac{sp}{m_{\mathrm{L}}}L_{\mathrm{LOS}}(r_i)\right)^{m_{\mathrm{L}}}}\right)^{K_{\mathrm{LOS}}}\right]\end{aligned} \tag{41}$$

and

$$\begin{aligned}\mathscr{L}_{I_{\mathrm{NLOS}}}[s] &= \mathbb{E}\left[\exp(-sI_{\mathrm{NLOS}})\right]\\ &= \mathbb{E}\left[\exp\left(-s\sum_{i\in\Phi_{\mathrm{NLOS}}\setminus\{b\}} pg_iL_{\mathrm{NLOS}}(r_i)\right)\right]\\ &= \mathbb{E}_{\Phi_{\mathrm{NLOS}}}\left[\prod_{i=1}^{K_{\mathrm{NLOS}}}\mathbb{E}_{g_i}\left[\exp\left(-spg_iL_{\mathrm{NLOS}}(r_i)\right)\right]\right]\\ &= \mathbb{E}_{\Phi_{\mathrm{NLOS}}}\left[\prod_{i=1}^{K_{\mathrm{NLOS}}}\frac{1}{1+spL_{\mathrm{NLOS}}(r_i)}\right]\\ &= \mathbb{E}_{r_i}\left[\left(\frac{1}{1+spL_{\mathrm{NLOS}}(r_i)}\right)^{K_{\mathrm{NLOS}}}\right]\end{aligned} \tag{42}$$

Hence, the LT of the aggregate interference under LOS and NLOS propagation are respectively given by

$$\begin{aligned}&\mathscr{L}_{I_{\mathrm{LOS}}}[s]\\ &= \int_r^{\mathsf{R}}\Pr[\mathrm{LOS}, r_i = y]\left(\frac{1}{\left(1+\frac{sp}{m_{\mathrm{L}}}L_{\mathrm{LOS}}(y)\right)^{m_{\mathrm{L}}}}\right)^{K_{\mathrm{LOS}}}\\ &\quad\times\frac{3\,y^2}{\mathsf{R}^3-r^3}\mathrm{d}y\end{aligned} \tag{43}$$

and

$$\begin{aligned}&\mathscr{L}_{I_{\mathrm{NLOS}}}[s]\\ &= \int_r^{\mathsf{R}}\Pr[\mathrm{NLOS}, r_i = y]\left(\frac{1}{1+spL_{\mathrm{NLOS}}(y)}\right)^{K_{\mathrm{NLOS}}}\\ &\quad\times\frac{3\,y^2}{\mathsf{R}^3-r^3}\mathrm{d}y.\end{aligned} \tag{44}$$

IV. NUMERICAL RESULTS

In this section, we analyze the performances of drone mobile networks under the path-loss based strategies. We provide some examples to varify the proposed analytical framework, and compare the Monte-Carlo simulations with theoretical results.

$$\begin{aligned}\mathcal{P}_{r_{\mathrm{NLOS,DM}}(t)}(w) &= \delta(w-\mathsf{D})\left(1+(\mathcal{H}(w-\mathsf{R})-1)\left(\frac{\mathsf{R}^3-(vt+w)^3}{\mathsf{R}^3-\mathsf{D}^3}\right)^{K_{\mathrm{NLOS}}}\right)+\mathcal{H}(w-\mathsf{D})\\ &\quad\times\left(\delta(w-\mathsf{R})\left(\frac{\mathsf{R}^3-(vt+w)^3}{\mathsf{R}^3-\mathsf{D}^3}\right)^{K_{\mathrm{NLOS}}}-\frac{3\,K_{\mathrm{NLOS}}(\mathcal{H}(w-\mathsf{R})-1)(vt+w)^2}{\mathsf{R}^3-\mathsf{D}^3}\left(\frac{\mathsf{R}^3-(tv+w)^3}{\mathsf{R}^3-\mathsf{D}^3}\right)^{K_{\mathrm{NLOS}}-1}\right).\end{aligned} \tag{31}$$

$$\begin{aligned}&\mathbb{E}[\log(1+\mathrm{SINR})]\\ &= \int_0^{+\infty}\Pr\left[\log(1+\mathrm{SINR})>\gamma\right]\mathrm{d}\gamma\\ &= \mathbb{E}_{r_b}\left[\int_0^{+\infty}\Pr[\mathrm{LOS}, r_b=r]\Pr[\log(1+\mathrm{SINR})>\gamma|r_b=r]+\Pr[\mathrm{NLOS}, r_b=r]\Pr[\log(1+\mathrm{SINR})>\gamma|r_b=r]\mathrm{d}\gamma\right]\\ &= \int_0^{\mathsf{R}}\int_0^{+\infty}\Pr[\mathrm{LOS}, r_b=r]\frac{1-\mathcal{F}_{\mathrm{SINR}|r_b=r}[\gamma]}{1+\gamma}\mathcal{P}_{r_b}(r)+\Pr[\mathrm{NLOS}, r_b=r]\frac{1-\mathcal{F}_{\mathrm{SINR}|r_b=r}[\gamma]}{1+\gamma}\mathcal{P}_{r_b}(r)\,\mathrm{d}\gamma\mathrm{d}r\end{aligned} \tag{35}$$

TABLE 1. Simulations parameters.

Parameter	Symbol	Value
Path-loss parameter in LOS link	α_{L}	3
Path-loss parameter in NLOS link	α_{N}	4
UAV Transmit power	p	20 W
Bandwidth	BW	20 MHz
Sphere radius	R	100 m
Critical distance	D	18 m
Carrier frequency	f_c	30 GHz

A. MONTE-CARLO SIMULATIONS

The method utilized for evaluating the spectral efficiency and outage probability in single-user multi-antenna drone mobile networks with CB using Monte-Carlo simulations are presented below.

1) Set the number of PPP deployment density λ, Nakagami-m fading parameter m_{L} and m_{N}, serving drone velocity v, transmit power p, number of antennas M, path-loss exponent α_{L}, α_{N}, and noise variance σ^2.
2) Define the 3D finite region radius R around the typical user o located at the origin and the critical distance D.
3) Generate the statistical number of LOS drone and NLOS drone using Poisson distribution with average $\bar{K}_{\mathrm{LOS}} = \frac{4}{3}\pi \mathsf{D}^3\lambda$ and $\bar{K}_{\mathrm{NLOS}} = \frac{4}{3}\pi\left(\mathsf{R}^3 - \mathsf{D}^3\right)\lambda$. Then, uniformly-deployed in the region of volume $\frac{4}{3}\pi\mathsf{D}^3$ and $\frac{4}{3}\pi\left(\mathsf{R}^3 - \mathsf{D}^3\right)$, respectively.
4) Generate independent fading channel power gains from all deployed drones to the typical user.
5) Associate the typical receiver to the nearest transmitter drone based on path-loss strategy. Then, the serving drone will move according to three mobility models, and the intended signal power X during the movement process can be obtained.
6) Calculate the aggregate network interference on the typical user I_{Iagg} using the sum of received signal powers from all remaining interfering links.
7) Obtain the instantaneous SINR and spectral efficiency (nat/s/Hz) of the typical receiver using $\mathrm{SINR} = \frac{X}{I_{\mathrm{Iagg}+\sigma^2}}$ and $\log(1+\mathrm{SINR})$, respectively.
8) By repeating the step 3-7 with a large number of times and calculating the averages, we can compute the spectral efficiency and outage probability.

Next, we will explain the theoretical results and Monte-Carlo simulations based on a standard workstations at present time. The execution time for Monte-Carlo simulations which were repeated 20k times over a radius of 100 m required can range from four hours to more than ten hours depending on the network settings. The deployment density, path-loss exponents, mobility model increase the complexity of the Monte-Carlo trials. However, with the presented theoretical framework, similar results can be obtained in few minutes. In this paper, all the parameters are set according to Table 1 unless otherwise stated in the subsequent results analysis. Furthermore, all the parameters in this section are merely chosen to illustrate the performance in an example, and it can be modified to any other values depending on the needs of different scenarios.

B. IMPACT OF NUMBER OF ANTENNAS

We investigate the effect of the number of antennas on the SE in Fig. 2. Here, we consider three mobility models, consisting (i) stationary model (red curves), (ii) deterministic mobility

$$
\begin{aligned}
\mathcal{F}_{\mathrm{SINR}|r_b=r}[\gamma] &= \Pr[\mathrm{LOS}, r_b = r]\Pr[\mathrm{SINR} \le \gamma|\mathrm{LOS}, r_b = r] \\
&\quad + \Pr[\mathrm{NLOS}, r_b = r]\Pr[\mathrm{SINR} \le \gamma|\mathrm{NLOS}, r_b = r] \\
&= 1 - \Pr[\mathrm{LOS}, r_b = r]\Pr[\mathrm{SINR} > \gamma|\mathrm{LOS}, r_b = r] \\
&\quad - \Pr[\mathrm{NLOS}, r_b = r]\Pr[\mathrm{SINR} > \gamma|\mathrm{NLOS}, r_b = r] \\
&= 1 - \Pr[\mathrm{LOS}, r_b = r]\Pr\left[g_b > \frac{\gamma}{pL_{\mathrm{LOS}}(r)}\left(I_{\mathrm{LOS}} + I_{\mathrm{NLOS}} + \sigma^2\right)|\mathrm{LOS}, r_o = r\right] \\
&\quad - \Pr[\mathrm{NLOS}, r_b = r]\Pr\left[g_b > \frac{\gamma}{pL_{\mathrm{NLOS}}(r)}\left(I_{\mathrm{NLOS}} + \sigma^2\right)|\mathrm{NLOS}, r_o = r\right] \\
&\overset{(i)}{=} 1 - \Pr[\mathrm{LOS}, r_b = r]\sum_{n=0}^{m_{\mathrm{L}}M-1}\left\{\frac{(-s)^n}{n!}\frac{\mathrm{d}^n}{\mathrm{d}s^n}\exp\left(-s\sigma^2\right)\mathscr{L}_{I_{\mathrm{LOS}}}[s]\mathscr{L}_{I_{\mathrm{NLOS}}}[s]\right\}_{s=\frac{m_{\mathrm{L}}\gamma}{pL_{\mathrm{LOS}}(r)}} \\
&\quad - \Pr[\mathrm{NLOS}, r_b = r]\sum_{n=0}^{M-1}\left\{\frac{(-s)^n}{n!}\frac{\mathrm{d}^n}{\mathrm{d}s^n}\exp\left(-s\sigma^2\right)\mathscr{L}_{I_{\mathrm{NLOS}}}[s]\right\}_{s=\frac{\gamma}{pL_{\mathrm{NLOS}}(r)}} \qquad (39)
\end{aligned}
$$

$$
\begin{aligned}
\mathcal{F}_{\mathrm{SINR}}[\gamma] = 1 - \int_0^{\mathsf{R}}\Bigg(&\Pr[\mathrm{LOS}, r_b = r]\sum_{n=0}^{m_{\mathrm{L}}M-1}\left\{\frac{(-s)^n}{n!}\frac{\mathrm{d}^n}{\mathrm{d}s^n}\exp\left(-s\sigma^2\right)\mathscr{L}_{I_{\mathrm{LOS}}}[s]\mathscr{L}_{I_{\mathrm{NLOS}}}[s]\right\}_{s=\frac{m_{\mathrm{L}}\gamma}{pL_{\mathrm{LOS}}(r)}} \\
&+ \Pr[\mathrm{NLOS}, r_b = r]\sum_{n=0}^{M-1}\left\{\frac{(-s)^n}{n!}\frac{\mathrm{d}^n}{\mathrm{d}s^n}\exp\left(-s\sigma^2\right)\mathscr{L}_{I_{\mathrm{NLOS}}}[s]\right\}_{s=\frac{\gamma}{pL_{\mathrm{NLOS}}(r)}}\Bigg)\mathcal{P}_{r_b}(r)\mathrm{d}r \qquad (40)
\end{aligned}
$$

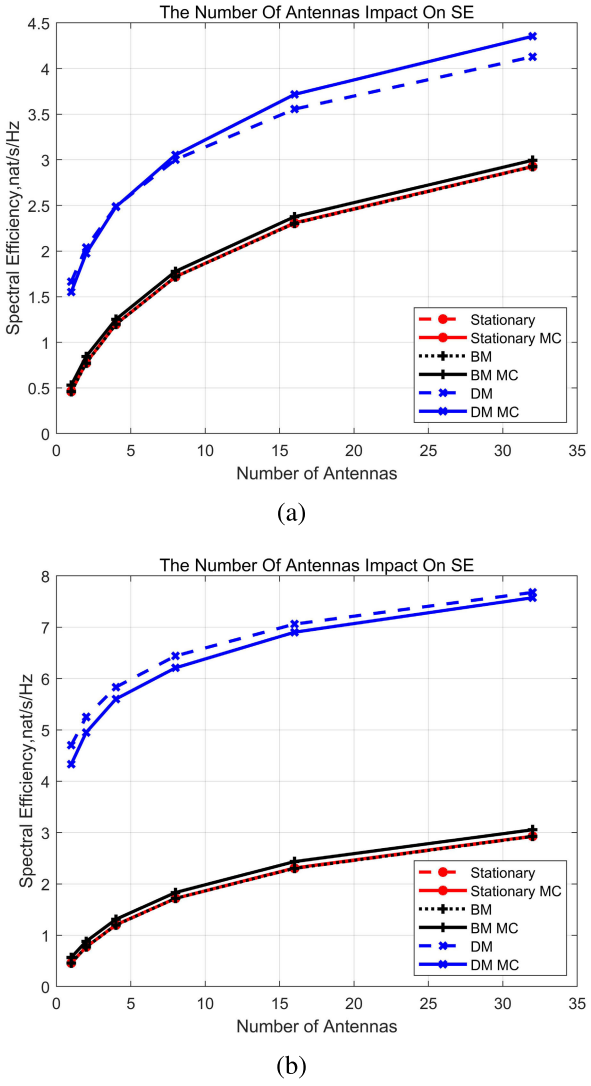

FIGURE 2. Spectral efficiency against different number of antennas. System parameters are: $m_{\mathrm{L}} = 3$, $m_{\mathrm{N}} = 1$, R = 100 m, D = 18 m, $\lambda = 10^{-5}$ $/m^3$, $v = 3$ m/s, $p = 20$ W, $\epsilon = \epsilon_{\mathrm{LOS}} = 1$ dB, $\epsilon = \epsilon_{\mathrm{NLOS}} = 20$ dB. (a) Time $t = 1$ s. (b) Time $t = 3$ s.

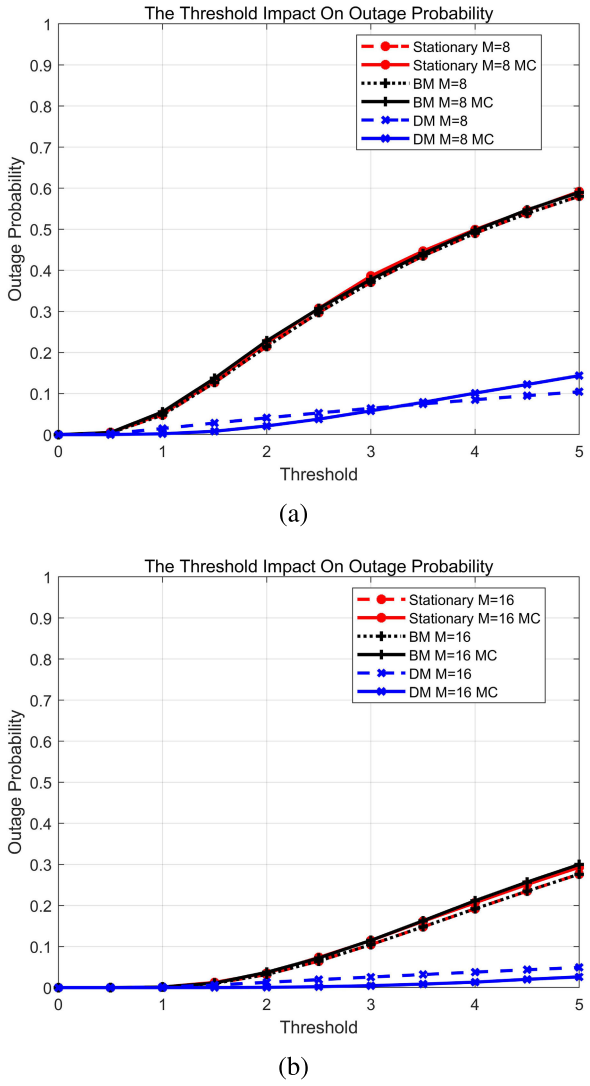

FIGURE 3. Outage probability against threshold with different number of antennas. System parameters are: $m_{\mathrm{L}} = 3$, $m_{\mathrm{N}} = 1$, R = 100 m, D = 18 m, $\lambda = 10^{-5}$ $/m^3$, $v = 3$ m/s, $p = 20$ W, $t = 3$ s, $\epsilon = \epsilon_{\mathrm{LOS}} = 1$ dB, $\epsilon = \epsilon_{\mathrm{NLOS}} = 20$ dB. (a) Number of antennas M = 8. (b) Number of antennas M = 16.

model (blue curves), and (iii) 3D Brownian mobility model (black curves). In order to compare the network performances at different time, we obtain the SE values at time $t = 1$ s and $t = 3$ s with different mobility models, respectively. The reason is because the serving drone is just starting to move according mobility models at time $t = 1$ s, and the drone mobile networks will have a better network performance at time $t = 3$ s. As it can been seen in Fig. 2(a) and Fig. 2(b), the SE performance in all mobility models always increases in the number of antennas. Furthermore, our findings show that drone mobile networks applied CB can obtain a better performance with more transmit antennas. Next, the effect of connecting threshold on outage probability with 8 and 16 antennas are investigated in Fig. 3(a) and Fig. 3(b), respectively. We can observe that the outage probability will increase and become stable with the increasing of threshold in all mobility models. The reason is because the serving drone will change to LOS condition under deterministic mobility model at time $t = 3$ s, but the serving drone still under NLOS condition in other mobility models. It is important to note that communicate under LOS condition can enhance the network performance. In addition, it can be observed that the outage probability performance under $M = 16$ is better than $M = 8$, that phenomenon fits the conclusion in Fig. 2. In Fig. 2 and Fig. 3, we can observe that the multi-antenna communications will increase the drone mobile performances. The reason is because the multi-antenna communications will improve the channel power gain, and hence, the useful signal power will stronger, whilst the interference level still remaining same. This trend highlights the important role of multi-antenna in

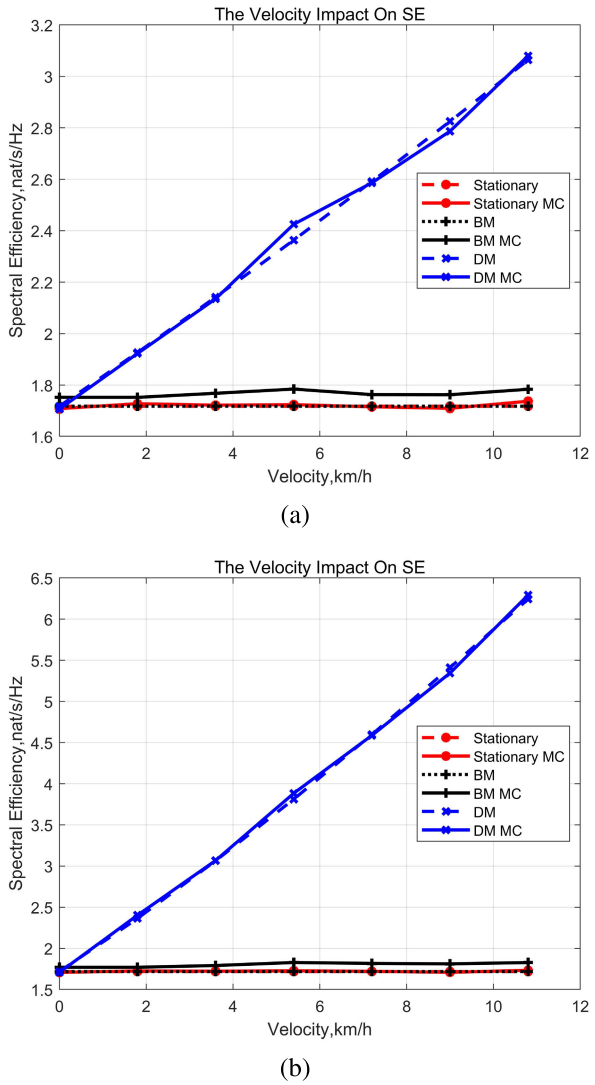

FIGURE 4. The serving drone velocity impact on Spectral efficiency. System parameters are: $M = 8$, $m_L = 3$, $m_N = 1$, R = 100 m, D = 18 m, $\lambda = 10^{-5}\ /m^3$, $p = 20$ W, $\epsilon = \epsilon_{LOS} = 1$ dB, $\epsilon = \epsilon_{NLOS} = 20$ dB. (a) Time $t = 1$ s. (b) Time $t = 3$ s.

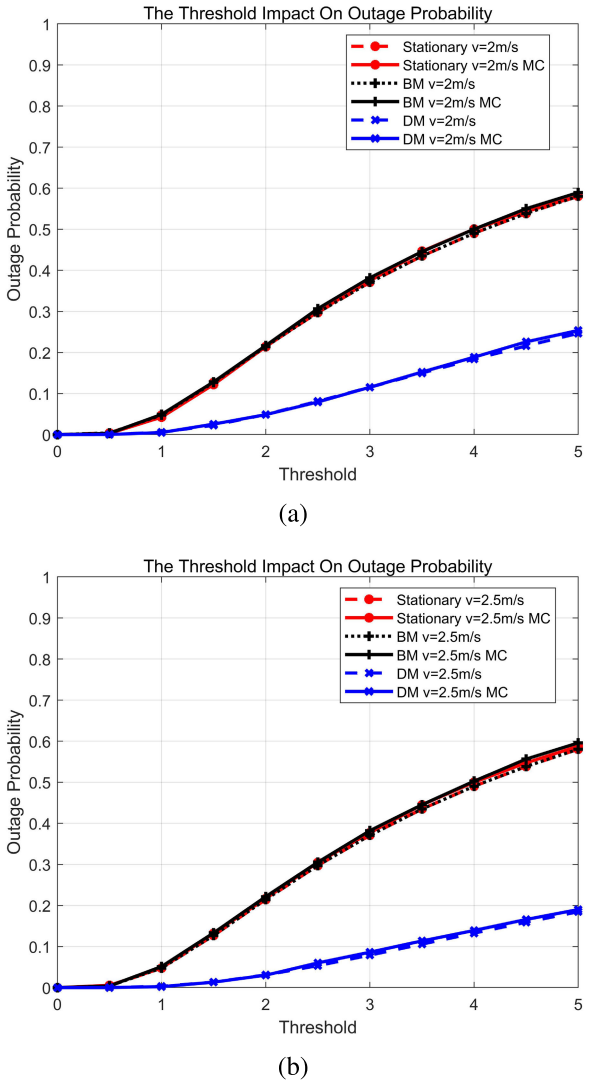

FIGURE 5. The threshold impact on Outage probability with different serving drone velocities. System parameters are: $M = 8$, $m_L = 3$, $m_N = 1$, R = 100 m, D = 18 m, $\lambda = 10^{-5}\ /m^3$, $p = 20$ W, $t = 3$ s, $\epsilon = \epsilon_{LOS} = 1$ dB, $\epsilon = \epsilon_{NLOS} = 20$ dB. (a) serving drone velocity $v = 2$ m/s. (b) serving drone velocity $v = 2.5$ m/s.

the drone mobile networks. In addition, it should be noted that 3D BM is the disordered mobility model, and deterministic motion is the ideal mobility model, in practical. So we can say that the performance of 3D BM is the lower bound of the reality drone networks and the performance of deterministic model is the upper bound. This conclusion will help to simplify the drone mobile networks in practical (i.e, Markov-motion model).

C. IMPACT OF DRONE VELOCITY

The effect of the serving drone velocity on SE under three mobility models at time $t = 1$ and time $t = 3$ are demonstrated in Fig. 4(a) and Fig. 4(b). As we can find that the SE under deterministic mobility model increase in the serving drone velocity, but the velocity has little impact on SE under stationary and 3D BM model. Depending on the characteristics of different mobility models, the distance between typical user and serving drone will decrease with the increasing of serving drone velocity. On the other hand, it is important to note that the distance has little change under stationary and 3D BM model. We depict the impact of connecting threshold on outage probability with $v = 7.2$ km/h and $v = 9$ km/h in Fig. 5(a) and Fig. 5(b). As expected, the velocity of drones will increase the drone mobile performances. Although the serving drone velocity will enhance the performance of drone mobile networks in practical, but it should be noted that strike a balance between secure and performance. However, this beyond the scope of this article.

D. IMPACT OF TRANSMITTER POWER

Finally, we proceed by studying the effect of transmitter power on SE under three mobility models in Fig. 6.

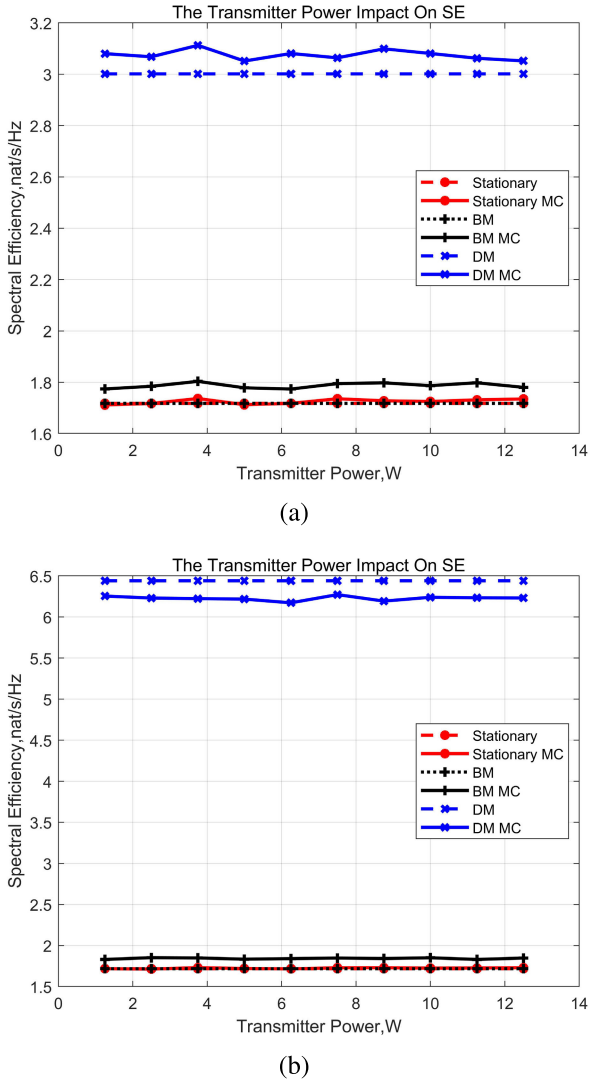

FIGURE 6. **The transmitter power impact on Spectral efficiency. System parameters are: $M = 8$, $m_L = 3$, $m_N = 1$, R = 100 m, D = 18 m, $\lambda = 10^{-5}$ $/m^3$, $v = 3$ m/s, $\epsilon = \epsilon_{LOS} = 1$ dB, $\epsilon = \epsilon_{NLOS} = 20$ dB. (a) Time $t = 1$ s. (b) Time $t = 3$ s.**

As expected, we can observe that the transmitter power has little impact on SE. The reason is because the intended signal power improve with the increasing of transmitter power, but the aggregate interference power also increase. Furthermore, it should be noted that the noise variance is small comparing with intended signal and aggregate interference, so the spectral efficiency and outage probability will remain stable at different transmit power. Hence, we can effectively allocate the limited energy of battery to other requirements to boost the overall performance of drone mobile networks in practical.

V. CONCLUSION

In this paper, a system-level analysis of the drone mobile networks is presented. Aiming to provide meaningful insights into the performance drone mobile networks in practice, we provided a framework for the study of mobile drone networks considering a number of mobility models, including a 3D Brownian motion model. Then, the expressions of SINR, spectral efficiency and coverage probability are obtained by using mathematical tools provided by stochastic geometry. Furthermore, a novel bounded formulations are given towards computing a lower-bound and upper-bound for the spectral efficiency and outage probability of the considered drone mobile networks. The Monte-Carlo simulation results validate the theoretical derivation and confirm the feasibility of a number of proposed mobility models. As for future work, one direction is to combine NOMA and full-duplex to improve the performances of drone mobile networks. Another direction is to evaluate and optimize the energy efficiency for drone mobile networks with considerations of simultaneous wireless information and power transfer (SWIPT). In addition, the performance of drone mobile networks considering shadowing and terrestrial base stations is worth being developed to satisfy the demands of wireless networks.

REFERENCES

[1] E. Turgut and M. C. Gursoy, "Downlink analysis in unmanned aerial vehicle (UAV) assisted cellular networks with clustered users," *IEEE Access*, vol. 6, pp. 36313–36324, 2018.

[2] B. Mukherjee, M. F. Habib, and F. Dikbiyik, "Network adaptability from disaster disruptions and cascading failures," *IEEE Commun. Mag.*, vol. 52, no. 5, pp. 230–238, May 2014.

[3] M. Mozaffari, W. Saad, M. Bennis, Y.-H. Nam, and M. Debbah, "A tutorial on UAVs for wireless networks: Applications, challenges, and open problems," *IEEE Commun. Surveys Tuts.*, vol. 21, no. 3, pp. 2334–2360, 3rd Quart., 2019.

[4] A. M. Hayajneh, S. A. R. Zaidi, D. C. McLernon, M. Di Renzo, and M. Ghogho, "Performance analysis of UAV enabled disaster recovery networks: A stochastic geometric framework based on cluster processes," *IEEE Access*, vol. 6, pp. 26215–26230, 2018.

[5] B. Galkin, J. Kibilda, and L. A. DaSilva, "A stochastic model for UAV networks positioned above demand hotspots in urban environments," *IEEE Trans. Veh. Technol.*, vol. 68, no. 7, pp. 6985–6996, Jul. 2019.

[6] W. Guo, C. Devine, and S. Wang, "Performance analysis of micro unmanned airborne communication relays for cellular networks," in *Proc. 9th Int. Symp. Commun. Syst., Netw. Digit. Sign (CSNDSP)*, Jul. 2014, pp. 658–663.

[7] S. D. Muruganathan, X. Lin, H.-L. Maattanen, J. Sedin, Z. Zou, W. A. Hapsari, and S. Yasukawa, "An overview of 3GPP release-15 study on enhanced LTE support for connected drones," 2018, *arXiv:1805.00826*. [Online]. Available: http://arxiv.org/abs/1805.00826

[8] A. Al-Hourani, S. Kandeepan, and A. Jamalipour, "Stochastic geometry study on device-to-device communication as a disaster relief solution," *IEEE Trans. Veh. Technol.*, vol. 65, no. 5, pp. 3005–3017, May 2016.

[9] L. Zhou, F. Luan, S. Zhou, A. F. Molisch, and F. Tufvesson, "Geometry-based stochastic channel model for high-speed railway communications," *IEEE Trans. Veh. Technol.*, vol. 68, no. 5, pp. 4353–4366, May 2019.

[10] G. A. Karagiannis, A. D. Panagopoulos, and J. D. Kanellopoulos, "Multidimensional rain attenuation stochastic dynamic modeling: Application to earth–space diversity systems," *IEEE Trans. Antennas Propag.*, vol. 60, no. 11, pp. 5400–5411, Nov. 2012.

[11] C. Fan, T. Zhang, Y. Liu, and Z. Zeng, "Cache-enabled HetNets with limited backhaul: A stochastic geometry model," *IEEE Trans. Commun.*, vol. 68, no. 11, pp. 7007–7022, Nov. 2020.

[12] Z. Zhang, Y. Li, K. Huang, S. Zhou, and J. Wang, "Energy efficiency analysis of cellular networks with cooperative relays via stochastic geometry," *China Commun.*, vol. 12, no. 9, pp. 112–121, 2015.

[13] J. Liu, G. Wu, X. Zhang, S. Fang, and S. Li, "Modeling, analysis, and optimization of grant-free NOMA in massive MTC via stochastic geometry," 2020, *arXiv:2004.02171*. [Online]. Available: http://arxiv.org/abs/2004.02171

[14] Z. Mobini, M. Mohammadi, B. K. Chalise, H. A. Suraweera, and Z. Ding, "Beamforming design and performance analysis of full-duplex cooperative NOMA systems," *IEEE Trans. Wireless Commun.*, vol. 18, no. 6, pp. 3295–3311, Jun. 2019.
[15] W. Tang, H. Zhang, and Y. He, "Tractable modelling and performance analysis of UAV networks with 3D blockage effects," *IEEE Wireless Commun. Lett.*, vol. 9, no. 12, pp. 2064–2067, Dec. 2020.
[16] Z. H. E. Tan, A. Madhukumar, R. P. Sirigina, and A. K. Krishna, "NOMA-aided multi-UAV communications in full-duplex heterogeneous networks," *IEEE Syst. J.*, vol. 15, no. 2, pp. 2755–2766, Jun. 2020.
[17] P. S. Bithas, V. Nikolaidis, A. G. Kanatas, and G. K. Karagiannidis, "UAV-to-ground communications: Channel modeling and UAV selection," *IEEE Trans. Commun.*, vol. 68, no. 8, pp. 5135–5144, Aug. 2020.
[18] T. Z. H. Ernest, A. S Madhukumar, R. P. Sirigina, and A. K. Krishna, "NOMA-aided UAV communications over correlated rician shadowed fading channels," *IEEE Trans. Signal Process.*, vol. 68, pp. 3103–3116, 2020.
[19] C. You and R. Zhang, "Hybrid offline-online design for UAV-enabled data harvesting in probabilistic LoS channels," *IEEE Trans. Wireless Commun.*, vol. 19, no. 6, pp. 3753–3768, Jun. 2020.
[20] C.-H. Liu, D.-C. Liang, M. A. Syed, and R.-H. Gau, "A 3D tractable model for UAV-enabled cellular networks with multiple antennas," *IEEE Trans. Wireless Commun.*, vol. 20, no. 6, pp. 3538–3554, Jun. 2021.
[21] C. K. Armeniakos, P. S. Bithas, and A. G. Kanatas, "SIR analysis in 3D UAV networks: A stochastic geometry approach," *IEEE Access*, vol. 8, pp. 204963–204973, 2020.
[22] H. Chang, C.-X. Wang, Y. Liu, J. Huang, J. Sun, W. Zhang, and X. Gao, "A novel nonstationary 6G UAV-to-ground wireless channel model with 3-D arbitrary trajectory changes," *IEEE Internet Things J.*, vol. 8, no. 12, pp. 9865–9877, Jun. 2021.
[23] V. V. C. Ravi and H. S. Dhillon, "Downlink coverage probability in a finite network of unmanned aerial vehicle (UAV) base stations," in *Proc. IEEE 17th Int. Workshop Signal Process. Adv. Wireless Commun. (SPAWC)*, Jul. 2016, pp. 1–5.
[24] V. V. Chetlur and H. S. Dhillon, "Downlink coverage analysis for a finite 3-D wireless network of unmanned aerial vehicles," *IEEE Trans. Commun.*, vol. 65, no. 10, pp. 4543–4558, Oct. 2017.
[25] L. Zeng, X. Cheng, C.-X. Wang, and X. Yin, "A 3D geometry-based stochastic channel model for UAV-MIMO channels," in *Proc. IEEE Wireless Commun. Netw. Conf. (WCNC)*, Mar. 2017, pp. 1–5.
[26] B. Galkin, J. Kibilda, and L. A. DaSilva, "Coverage analysis for low-altitude UAV networks in urban environments," in *Proc. GLOBECOM-IEEE Global Commun. Conf.*, Dec. 2017, pp. 1–6.
[27] M. Mozaffari, W. Saad, M. Bennis, and M. Debbah, "Unmanned aerial vehicle with underlaid device-to-device communications: Performance and tradeoffs," *IEEE Trans. Wireless Commun.*, vol. 15, no. 6, pp. 3949–3963, Jun. 2016.
[28] J. Lyu, Y. Zeng, and R. Zhang, "Spectrum sharing and cyclical multiple access in UAV-aided cellular offloading," in *Proc. GLOBECOM-IEEE Global Commun. Conf.*, Dec. 2017, pp. 1–6.
[29] S. Zhang and J. Liu, "Analysis and optimization of multiple unmanned aerial vehicle-assisted communications in post-disaster areas," *IEEE Trans. Veh. Technol.*, vol. 67, no. 12, pp. 12049–12060, Dec. 2018.
[30] W. Yi, Y. Liu, A. Nallanathan, and G. K. Karagiannidis, "A unified spatial framework for clustered UAV networks based on stochastic geometry," in *Proc. IEEE Global Commun. Conf. (GLOBECOM)*, Dec. 2018, pp. 1–6.
[31] H. Wu, X. Tao, N. Zhang, and X. Shen, "Cooperative UAV cluster-assisted terrestrial cellular networks for ubiquitous coverage," *IEEE J. Sel. Areas Commun.*, vol. 36, no. 9, pp. 2045–2058, Sep. 2018.
[32] M. Alzenad and H. Yanikomeroglu, "Coverage and rate analysis for unmanned aerial vehicle base stations with LoS/NLoS propagation," in *Proc. IEEE Globecom Workshops (GC Wkshps)*, Dec. 2018, pp. 1–7.
[33] W. Bao and B. Liang, "Stochastic geometric analysis of user mobility in heterogeneous wireless networks," *IEEE J. Sel. Areas Commun.*, vol. 33, no. 10, pp. 2212–2225, Oct. 2015.
[34] S. Choi, J.-G. Choi, and S. Bahk, "Mobility-aware analysis of millimeter wave communication systems with blockages," *IEEE Trans. Veh. Technol.*, vol. 69, no. 6, pp. 5901–5912, Jun. 2020.
[35] X. Xu, Y. Zhang, Z. Sun, Y. Hong, and X. Tao, "Analytical modeling of mode selection for moving D2D-enabled cellular networks," *IEEE Commun. Lett.*, vol. 20, no. 6, pp. 1203–1206, Jun. 2016.
[36] M. Farokhi, A. Zolghadrasli, and N. M. Yamchi, "Mobility-based cell and resource allocation for heterogeneous ultra-dense cellular networks," *IEEE Access*, vol. 6, pp. 66940–66953, 2018.
[37] H. Tabassum, M. Salehi, and E. Hossain, "Fundamentals of mobility-aware performance characterization of cellular networks: A tutorial," *IEEE Commun. Surveys Tuts.*, vol. 21, no. 3, pp. 2288–2308, 3rd Quart., 2019.
[38] S. N. Chiu, D. Stoyan, W. S. Kendall, and J. Mecke, *Stochastic Geometry and Its Applications*. Hoboken, NJ, USA: Wiley, 2013.
[39] A. Shojaeifard, K.-K. Wong, M. Di Renzo, G. Zheng, K. A. Hamdi, and J. Tang, "Full-duplex versus half-duplex large scale antenna system," in *Proc. IEEE Int. Conf. Commun. Workshops (ICC Workshops)*, May 2017, pp. 743–748.
[40] A. Shojaeifard, K.-K. Wong, M. Di Renzo, G. Zheng, K. A. Hamdi, and J. Tang, "Massive MIMO-enabled full-duplex cellular networks," *IEEE Trans. Commun.*, vol. 65, no. 11, pp. 4734–4750, Nov. 2017.
[41] A. Al-Hourani, S. Kandeepan, and A. Jamalipour, "Modeling air-to-ground path loss for low altitude platforms in urban environments," in *Proc. IEEE Global Commun. Conf. (GLOBECOM)*, Dec. 2014, pp. 2898–2904.
[42] N. Rupasinghe, Y. Yapici, I. Guvenc, and Y. Kakishima, "Non-orthogonal multiple access for mmWave drone networks with limited feedback," *IEEE Trans. Commun.*, vol. 67, no. 1, pp. 762–777, Jan. 2019.
[43] J. Arnau, I. Atzeni, and M. Kountouris, "Impact of LOS/NLOS propagation and path loss in ultra-dense cellular networks," in *Proc. IEEE Int. Conf. Commun. (ICC)*, May 2016, pp. 1–6.
[44] I. Atzeni, J. Arnau, and M. Kountouris, "Downlink cellular network analysis with LOS/NLOS propagation and elevated base stations," *IEEE Trans. Wireless Commun.*, vol. 17, no. 1, pp. 142–156, Jan. 2018.
[45] J. Huang, A. Shojaeifard, J. Tang, and K.-K. Wong, "System-level performance analysis in 3D drone mobile networks," in *6GN for Future Wireless Networks*, X. Wang, V. C. M. Leung, K. Li, H. Zhang, X. Hu, and Q. Liu, Eds., Cham, Switzerland: Springer, 2020, pp. 311–322.
[46] S. Srinivasa and M. Haenggi, "Distance distributions in finite uniformly random networks: Theory and applications," *IEEE Trans. Veh. Technol.*, vol. 59, no. 2, pp. 940–949, Feb. 2010.
[47] P. Kumaraswamy, "A generalized probability density function for double-bounded random processes," *J. Hydrol.*, vol. 46, nos. 1–2, pp. 79–88, Mar. 1980.
[48] J. Park, S. Y. Jung, S.-L. Kim, M. Bennis, and M. Debbah, "User-centric mobility management in ultra-dense cellular networks under spatio-temporal dynamics," in *Proc. IEEE Global Commun. Conf. (GLOBECOM)*, Dec. 2016, pp. 1–6.
[49] S. Miller and D. Childers, *Probability and Random Processes: With Applications to Signal Processing and Communications*. New York, NY, USA: Academic, 2012.
[50] A. Alammouri, J. G. Andrews, and F. Baccelli, "A unified asymptotic analysis of area spectral efficiency in ultradense cellular networks," *IEEE Trans. Inf. Theory*, vol. 65, no. 2, pp. 1236–1248, Feb. 2019.

JIAYI HUANG is currently pursuing the M.S. degree with the School of Electronic and Information Engineering, South China University of Technology, Guangzhou, China. His research interests include information theory and communications, physical layer security, and B5G networks.

JIE TANG (Senior Member, IEEE) received the B.Eng. degree in information engineering from the South China University of Technology, Guangzhou, China, in 2008, the M.Sc. degree (Hons.) in communication systems and signal processing from the University of Bristol, U.K., in 2009, and the Ph.D. degree from Loughborough University, Leicestershire, U.K., in 2012. From 2013 to 2015, he was a Research Associate with the School of Electrical and Electronic Engineering, The University of Manchester, U.K. He is currently a Full Professor with the School of Electronic and Information Engineering, South China University of Technology, China. His current research interests include 5G and beyond mobile communications, including topics such as massive MIMO, full-duplex communications, edge caching and fog networking, physical layer security, UAV communications, wireless power transfer, and mobile computing. He is a Senior Member of CIE and CIC. He has served as the Track Co-Chair for IEEE VTC-Spring 2018, EAI GreeNets 2019, ICCC 2019, and ICCC 2020. He was a co-recipient of the 2018 IEEE ICNC, 2018 CSPS, 2019 IEEE WCSP, and 2020 6GN Best Paper Awards. He has been serving as the Vice-Chair for IEEE SIG on green cellular networks and an Editor for IEEE Wireless Communications Letters, IEEE Systems Journal, IEEE Access, *Physical Communication*, and *EURASIP Journal on Wireless Communications and Networking*.

ARMAN SHOJAEIFARD (Senior Member, IEEE) received the B.Eng. degree in information systems engineering from the Imperial College London, in 2008, and the M.Sc. degree in signal processing (Hons.) and the Ph.D. degree in wireless communications from the King's College London, in 2009 and 2013, respectively. He is currently the Wireless Research Manager of BT Labs, where he leads the European CELTIC-NEXT Project on AI-enabled Massive MIMO (AIMM). He also represents BT as a Standardization Delegate at 3GPP RAN1 WG and O-RAN Alliance WG3. He previously held a Postdoctoral Research positions at the University College London and The University of Manchester. He is an Editor of IEEE Wireless Communications Letters and *Electronics Letters* (IET).

ZHEN CHEN (Member, IEEE) received the Ph.D. degree in signal and information processing from the South China University of Technology, Guangzhou, China, in 2019. From 2020 to 2021, he was a Research Fellow with the Hong Kong Applied Science and Technology Research Institute, Hong Kong. He was also a Visiting Scholar with the School of Software, Xiamen University, from 2014 to 2015. His research interests include compressed sensing, wireless communication, and medical image processing.

JUNCHENG HU received the B.Eng. degree in telecommunications engineering from the Hunan University of Science and Technology, Hunan, China, in 2007, and the M.Sc. degree in mobile communications engineering and the Ph.D. degree from Loughborough University, Leicestershire, U.K., in 2008 and 2013, respectively. From 2014 to 2017, he was a System Integration Engineer with CSE Transtel Pte., Ltd., SG. He is currently a Senior Lecturer with the School of Humanity and Management, Guilin Medical University, China. His current research interests include the application of big data of medical information and artificial intelligence of medical image in early screening for gastric cancer and myocardial infarction.

DANIEL KA CHUN SO (Senior Member, IEEE) received the B.Eng. degree (Hons.) in electrical and electronics engineering from The University of Auckland, New Zealand, and the Ph.D. degree in electrical and electronics engineering from The Hong Kong University of Science and Technology (HKUST). He joined The University of Manchester as a Lecturer, in 2003, where he is currently a Professor and the Discipline Head of education with the Department of Electrical and Electronic Engineering. His research interests include green communications, NOMA, beyond 5G and 6G networks, heterogeneous networks, SWIPT, massive MIMO, cognitive radio, D2D and cooperative communications, channel equalization, and estimation techniques. He has served as the Symposium Co-Chair for IEEE ICC 2019 and Globecom 2020 and the Track Co-Chair for IEEE Vehicular Technology Conference (VTC) Spring 2016, 2017, and 2018, and 2021. He is also the Current Chair of the Special Interest Group on Green Cellular Networks within the IEEE ComSoc Green Communications and Computing Technical Committee. He has been serving as a Senior Editor for IEEE Wireless Communications Letters after being an Editor from 2016 to 2020, and an Editor for IEEE Transactions on Wireless Communications. He is the Lead Guest Editor of a Special Issue of IEEE Transactions on Green Communications and Networking, in 2021.

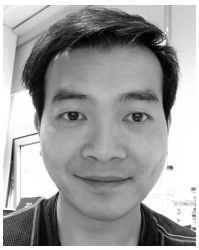

KAI-KIT WONG (Fellow, IEEE) received the B.Eng., M.Phil., and Ph.D. degrees in electrical and electronic engineering from The Hong Kong University of Science and Technology, Hong Kong, in 1996, 1998, and 2001, respectively. After graduation, he took up academic and research positions at The University of Hong Kong, Lucent Technologies, Bell-Labs, Holmdel, the Smart Antennas Research Group of Stanford University, and the University of Hull, U.K. He is currently the Chair of wireless communications at the Department of Electronic and Electrical Engineering, University College London, U.K. His current research interests include 5G and beyond mobile communications. He is a Fellow of IET and is also on the editorial board of several international journals. He was a co-recipient of the 2013 IEEE Signal Processing Letters Best Paper Award and the 2000 IEEE VTS Japan Chapter Award at the IEEE Vehicular Technology Conference, Japan, in 2000, and a few other international best paper awards. He has been the Editor-in-Chief of IEEE Wireless Communications Letters since 2020.